Supplementary Material 1 for:

Successional stages of methane seep systems off central Chile: linking active sediment-hosted seepage with long-lived carbonate chemoherms

Tina Treude[1], Peter Linke[2], Volker Liebetrau[2†], Florian Scholz[3], Philip Steeb[2], Jacob Geersen[4], Mark Schmidt[2], Stefan Sommer[2], Lorenzo Rovelli[5], Lee Bryant[6], and Jan Scholten[7]

[1]University of California - Los Angeles, Earth, Planetary, and Space Science, Los Angeles, United States

[2]GEOMAR Helmholtz Centre for Ocean Research, Kiel, Germany

[3]Universität Hamburg, Department of Earth System Sciences, Hamburg, Germany

[4]Leibniz Institute for Baltic Sea Research Warnemünde, Rostock, Germany

[5]Federal Institute of Hydrology, Koblenz, Germany

[6]University of Bath, Climate Adaptation and Environment Research (CAER) Centre, Bath, UK

[7]Institute of Geosciences, Kiel University, Germany

Correspondence to: Tina Treude (ttreude@g.ucla.edu) and Peter Linke (plinke@geomar.de)

[†]Deceased

1. Supplementary Methods

1.1 Profiler Lander (PRFL)

1.1.1 Profile acquisition

Along each transect of vertical microsensor profiling, each profile acquisition consisted of two steps: (1) a fast-search, low-resolution, profile was performed in mm steps until the sediment-water interface (SWI) was detected, then the sensor array was retracted and moved 3 mm forward along the x-axis to where (2) the high-resolution profile was performed. High-resolution profiling was performed in 100-µm steps from a programmable 'safety distance' (19 mm) above the depth of the previously detected SWI to a pre-selected profile depth into the sediment (24 mm; thus, total profile length of 43 mm). After each successive profile, the sensor array was moved forward 16 mm along the x-axis. If the fast-search profile failed to detect the SWI, the array was set to again move forward 16 mm and perform another search profile.

1.1.2 Microsensors calibration and processing

Each O_2 profile was individually calibrated using a two-point method based on 1) O_2 concentrations in the oxic, well-mixed bottom water, as obtained from optode measurements at the beginning of each profile, and 2) zero-level O_2 concentrations (0 µmol L^{-1}) measured in the anoxic sediment at the end of each profile. Diffusive oxygen uptake (DOU) rates were calculated from the micro-profiles based on Fick's first law of diffusion in water (Jørgensen and Des Marais, 1990) as (Suppl. Eq 1):

$$DOU = -D_{O_2} \frac{\Delta O_2}{\delta_{DBL}} \quad (1)$$

with D_{O2} being the molecular diffusion coefficient of O_2 in seawater and $\Delta O_2 = C_{bulk} - C_{SWI}$ being the O_2 concentration difference between the SWI (C_{SWI}) and the upper boundary (C_{bulk}) of the diffusive boundary layer (DBL) following Jørgensen and Revsbech (1985). The upper DBL boundary was defined as the intersection of the linearly extrapolated concentration gradient within the DBL and C_{bulk} in the overlying water. The SWI was determined visually via identification of distinct changes in the slope in the O_2 concentration profiles as a result of shifts between D_{O2} in the overlying water and within porous media (Bryant et al., 2010; Jørgensen and Des Marais, 1990). The O_2 diffusion coefficient D_{O2}, 1.57 x 10^{-9} m^2 s^{-1} at 10°C (Broecker and Peng, 1974), was corrected for in situ temperature and salinity following the Einstein-Stokes relationship (Yuan-Hui and Gregory, 1974).

The H_2S sensors were calibrated using a sodium sulfide – sodium hydroxide stock solution paired with a pH 7 phosphate buffer solution. Based on selected dilutions of the stock-buffer solution, a four-point calibration was performed across the concentration range 3 – 31 µmol L^{-1} H_2S (PRFL-1) and 3 – 123

µmol L^{-1} H_2S (PRFL-2). The H_2S concentrations for each of the pH 7 dilutions were calculated from the total sulfide concentrations (ΣH_2S) as (Suppl. Eq. 2):

$$H_2S = \Sigma H_2S/(1 + 10^{-pK}/10^{-pH}) \quad (2)$$

with pK1 being the H_2S dissociation constant based on lab conditions, 21°C (Millero et al., 1988). A linear relationship was assumed between the sensor reading and the H_2S concentration (Jeroschewski et al., 1996).

In addition to O_2 and H_2S microsensors, a pH microsensor was used during the first Profiler deployment in Box-2, but it malfunctioned and was therefore not included in the second deployment. Corresponding pH values were instead measured independently using sediment cores.

1.1.3 Significance of DOU rates for habitat characterization

The influence of the deployment duration on the robustness of the obtained DOU rates was investigated by considering subsections of the overall transects. As each transect was programmed to perform 27 array profiles using two O_2 microsensors simultaneously, we were able to simulate any transect length from 1 profile to the whole 27-profile transect. For example, a transect of 12 profiles, which would require a 24-h deployment, can be simulated considering subsample profiles, starting from 1–12, 2–13, etc. and continuing until the last possible subsample, profiles 15–27. Note that only consecutive profiles were considered. Prior to statistical analysis, the DOU datasets were first transformed using the log transformation $y = ln(x)$ to reduce data skewness, following Stahel (2002). Normal distribution was tested for each subsample via the Lilliefors test at a 5% significance level. Any combination of PRFL-1 and PRFL-2 subsamples of equal length (i.e., same number of array profiles) was subsequently compared with an unpaired Student's t-test. The null hypothesis (H_0) is that there is no significant difference in the DOU distribution between PRFL-1 and PRFL-2. The results are presented as the percentage of habitat differentiation, defined as the percentage of subsample pairs for which the H_0 was rejected at the 5% significance level ($p < 0.05$) for each subsample length. A habitat differentiation of 100% means that PRFL-1 and PRFL-2 can always be statistically separated regardless of which subsamples are compared.

1.2 Eddy Correlation Module (ECM) data processing

For ECM analyses, acoustic Doppler velocimeter (ADV) data were averaged to 8 Hz and poor-quality flow data, as defined by beam correlation <50% and signal-to-noise ratio <10, were replaced via linear interpolation (Rovelli et al., 2015). Data outliers in both flow and O_2 time series were removed with the Despiking Toolbox (Mori et al., 2007) and the velocity coordinate system was rotated to minimize effects

of horizontal velocity projections on the vertical velocity (McGinnis et al., 2008). The coordinate rotation was performed using a planar-fit (e.g.,(Lorke et al., 2013)) to obtain a vertical velocity component perpendicular to the local flow plane.

Total O_2 uptake flux rates (F; mmol m^{-2} d^{-1}) were estimated using the Fortran suite Sulfide-Oxygen-Heat Flux Eddy Analysis (SOHFEA, version 2.0; McGinnis et al. (2014)) as (Suppl. Eq. 3):

$$F = \overline{w'C'} \quad (3)$$

with w' (cm s^{-1}) and C' (µmol L^{-1}) being the fluctuations of vertical velocity and O_2 concentration, respectively. The fluctuations were obtained via a running average, following Reynolds decomposition (Berg et al., 2003). The optimal window size of 5 min for the running average represented a compromise between including all turbulent contributions and excluding non-turbulent contributions; the optimal window size was identified based on incremental averaging of the ECM fluxes (Rovelli et al., 2015; Attard et al., 2015). The dataset was also time-shifted to account for possible misalignment between the O_2 and velocity time series resulting from both the O_2 microelectrode response time and water travel time between the microelectrode tip and ADV sampling volume (Donis et al., 2015). Fluxes obtained during periods with unstable flow conditions, e.g., sharp shifts in flow direction or insufficient flow for well-developed turbulence conditions, were flagged and discarded from further analysis, as in Rovelli et al. (2015).

To account for potential O_2 storage ($F_{storage}$) due to transient O_2 concentration changes in the water-column region between the sediment and the height (h) of the sampling volume for the turbulent ECM flux (F) measurements, benthic O_2 uptake rates ($F_{benthic}$) were estimated to account for an O_2 storage term, following parameterization by (Rheuban et al., 2014), as (Suppl. Eq. 4):

$$F_{benthic} = F + F_{storage} = F + \int_0^h \frac{dC}{dt} dz \quad (4)$$

with dC/dt being the temporal O_2 concentration gradient (in µmol L^{-1}- h^{-1}). An estimate of the seafloor area integrated by ECM flux measurements, termed 'footprint', was obtained from h paired with the mean sediment surface roughness parameter (z_0), following the empirical model proposed by Berg et al. (2007). Values of z_0 were calculated from friction velocity (u*) and Reynolds stress (Reidenbach et al., 2006; Inoue et al., 2011). See Supp. Material 1 Figs. 5 and 6 for $F_{benthic}$ estimates for Boxes 2 and 4, respectively.

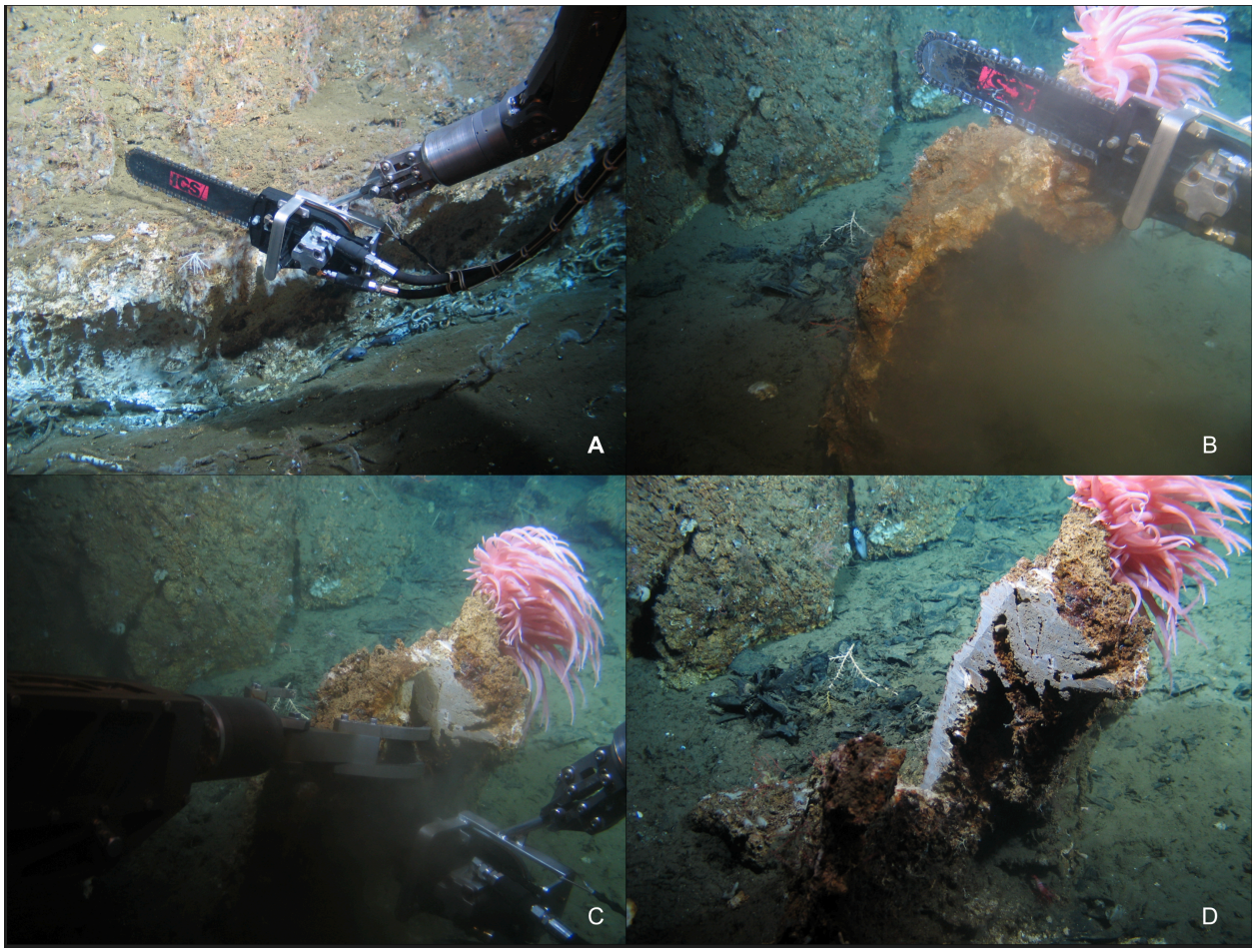
1.3 Theoretical particle tracks with the Paleo-Oceanography (POZ) lander

Theoretical particle tracks visualize the motion of water masses and their residence time within a specific region and thus provide a sense for the dispersion potential of solutes and suspended material. Three-dimensional current velocities obtained from an acoustic Doppler current profiler (ADCP, RD-Instruments, Poway, United States; attached to the POZ lander) were averaged from 1 min to 15 min, to reduce signal noise and minimize the effect of short-lived (single point) velocities spikes. Based on these average velocities, the location of a theoretical particle moving with the flow was iteratively computed assuming a constant velocity over each 15-min time step as (Suppl. Eq. 5):

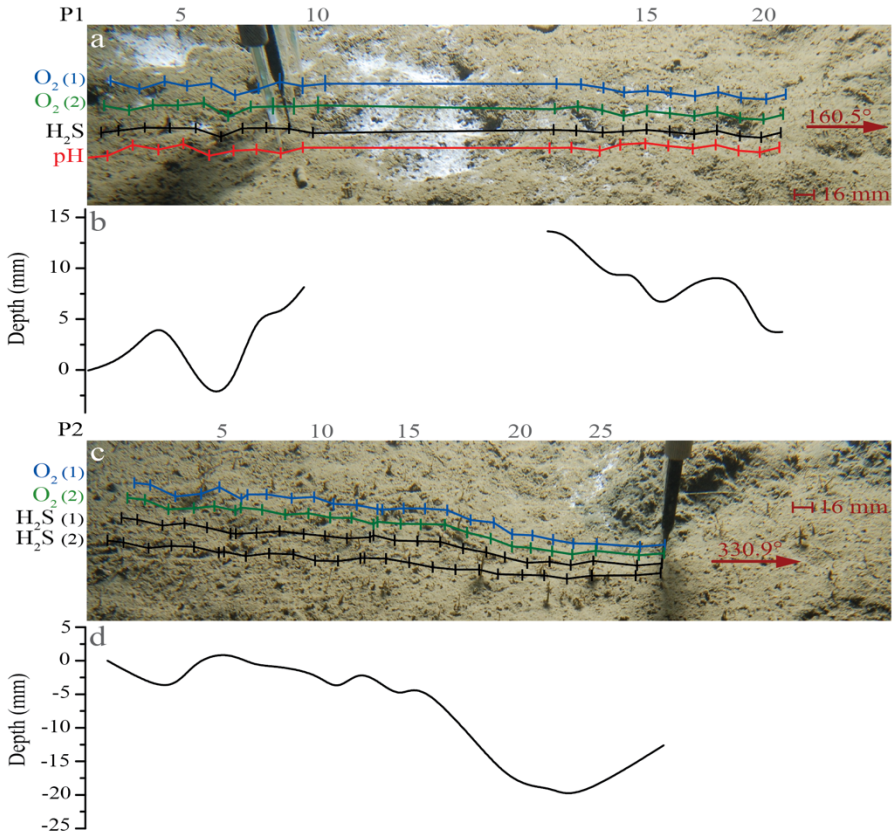
$$x(t) = x_0 + v_0 t \quad (5)$$

with *x(t)* being the east and north position over time, starting from the location x_0 (0,0), and v the average east and north velocity over the 15-min time step, with v_0 being the average velocity over the first 15-min time step. These calculations were performed for each ADCP bin and then averaged to the near-seafloor region within Boxes 2 and 4, i.e., distance from the seafloor from 2.1 to 21.6 m (POZ-1) and from 2.1 to 21.5 m (POZ-2), respectively. Averaging the calculations over the near-seafloor region allowed for smoothing of the particle tracks to facilitate better comparison of the flow dynamics between the near-seafloor regions of Boxes 2 and 4 (Supp. Material 1 Figure 7).

2. Supplementary Figures



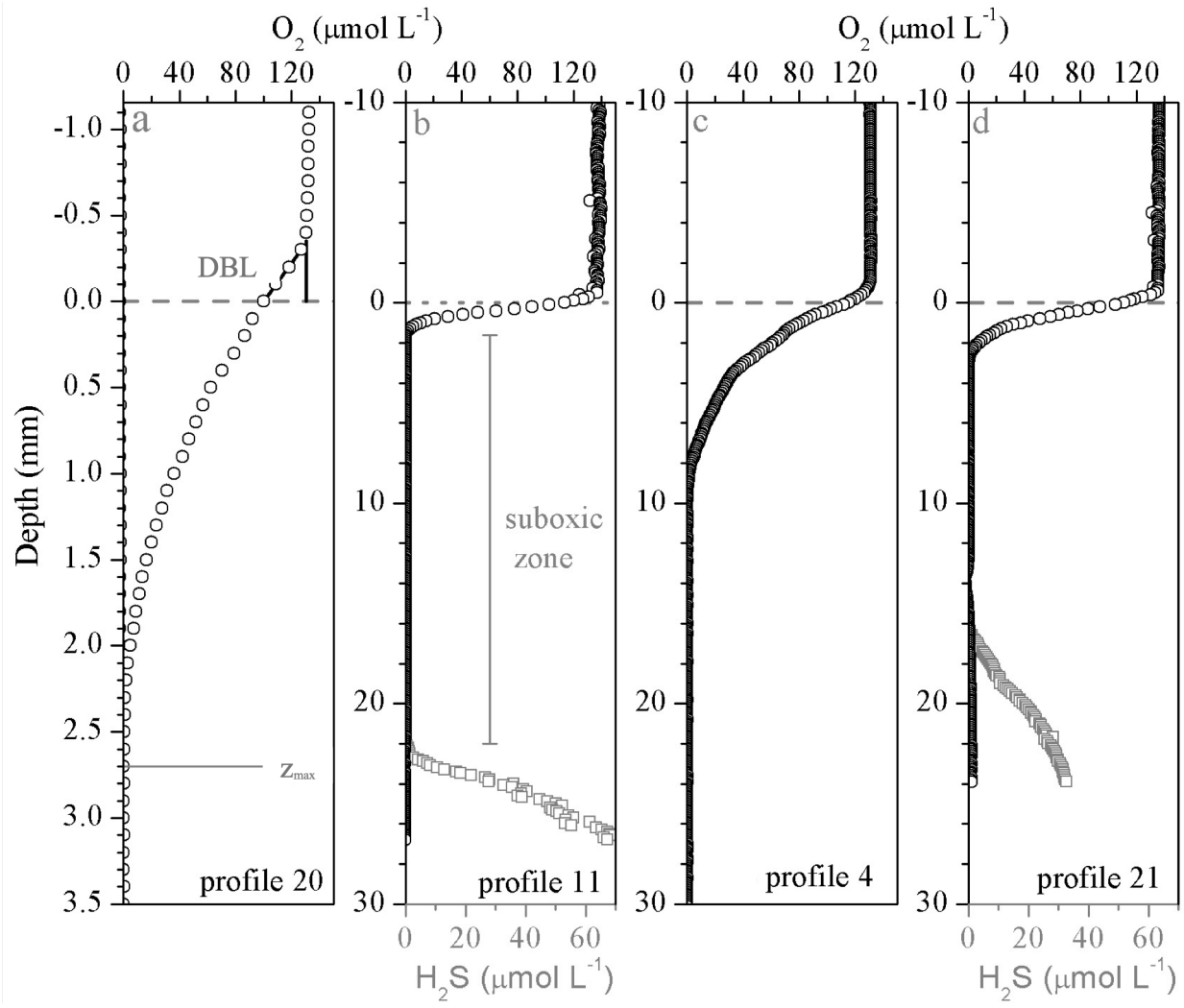
Supplementary Figure 1. (A) Underwater chainsaw (ICS Diamond Tools, Model 890F4) integrated into the remotely operated vehicle (ROV) Kiel 6000 hydraulic system and operated using the ORION manipulator during R/V SONNE expedition SO210. (B-D) Sequence of carbonate cutting and sampling: (B) Cutting carbonate with the chainsaw using the ORION manipulator, (C) sampling carbonate subsample with the RIGMASTER manipulator, (D) exposed cut area with intact anemone to the right.



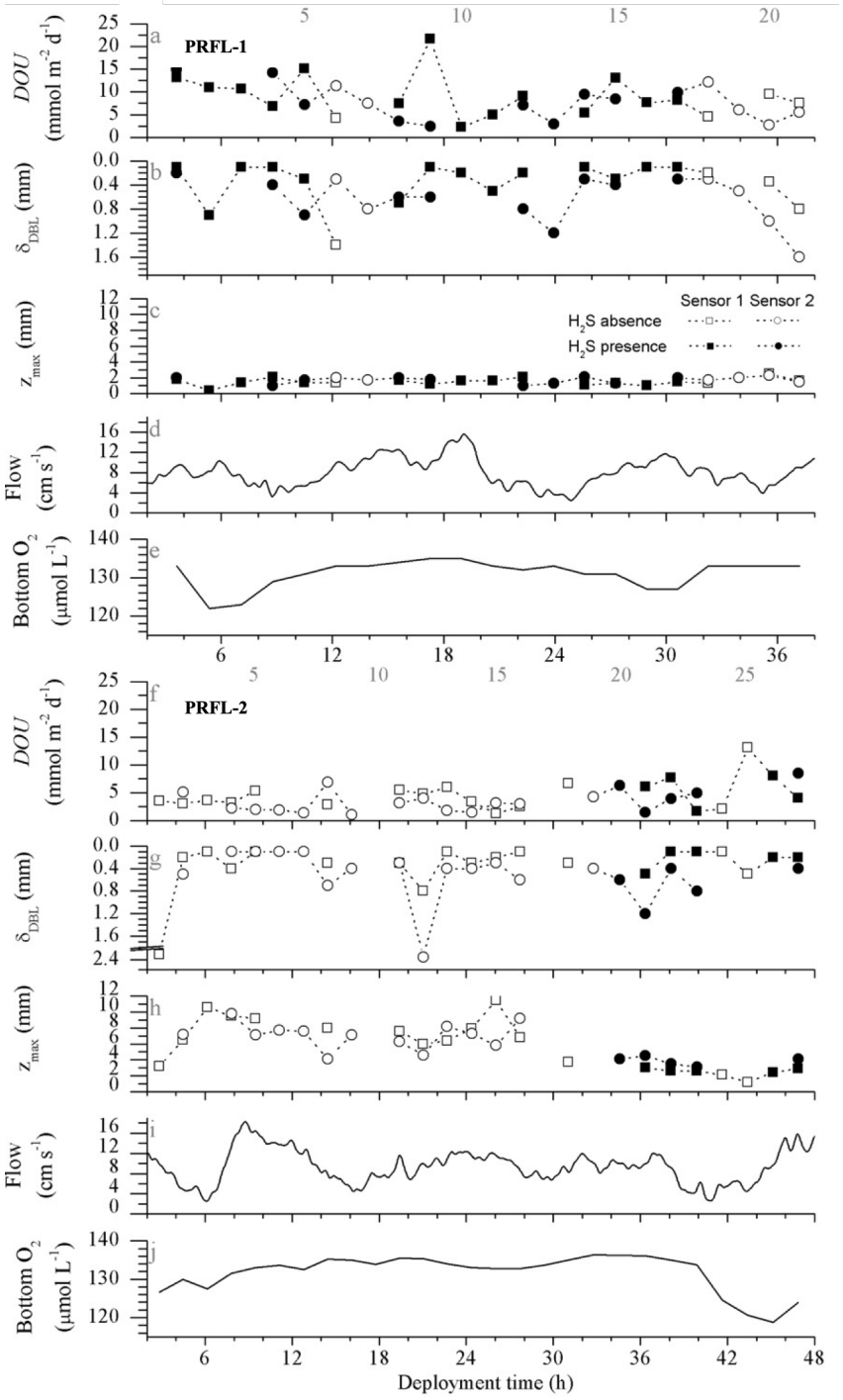
140

141 **Supplementary Figure 2. Transect images and corresponding elevation profiles for PRFL-1 (a, b) and PRFL-2**
142 **(c, d) in Box-2.** (a, c) Transect images overlaid with O_2, H_2S, and pH profiles; vertical bars mark individual profile
143 locations along the transect, arrows indicate the x-axis direction. (b, d) Elevation profiles derived from the
144 sediment–water interface (SWI) identified by O_2 sensors, with the SWI of profile 1 set to 0 mm. Due to a technical
145 malfunction, the step size between PRFL-1 profiles 10 and 11 exceeded the programmed 16 mm, leaving a 130 mm
146 gap in coverage. In PRFL-2, step sizes varied, with shorter spacing between profiles 6–7 and 13–14, and a larger
147 step between profiles 26–27.

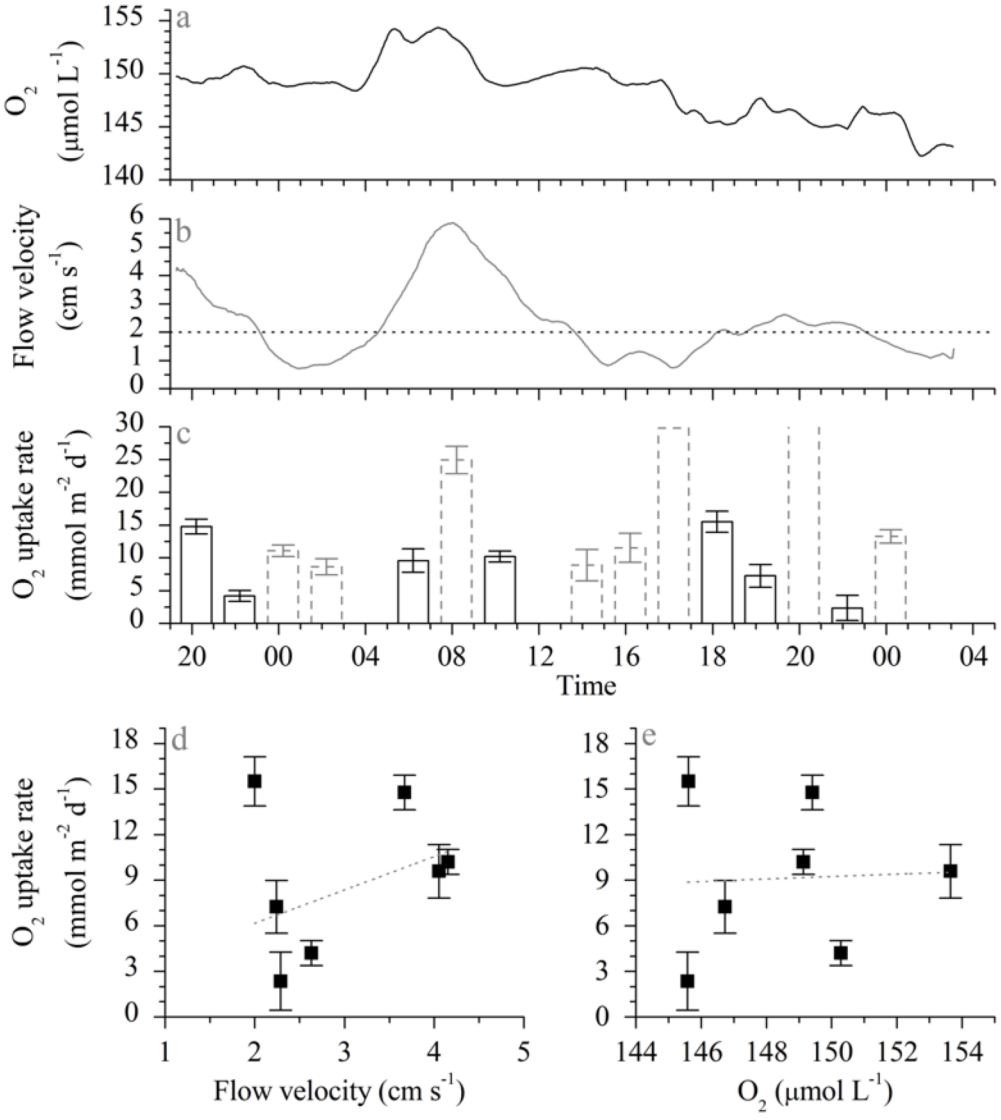
148



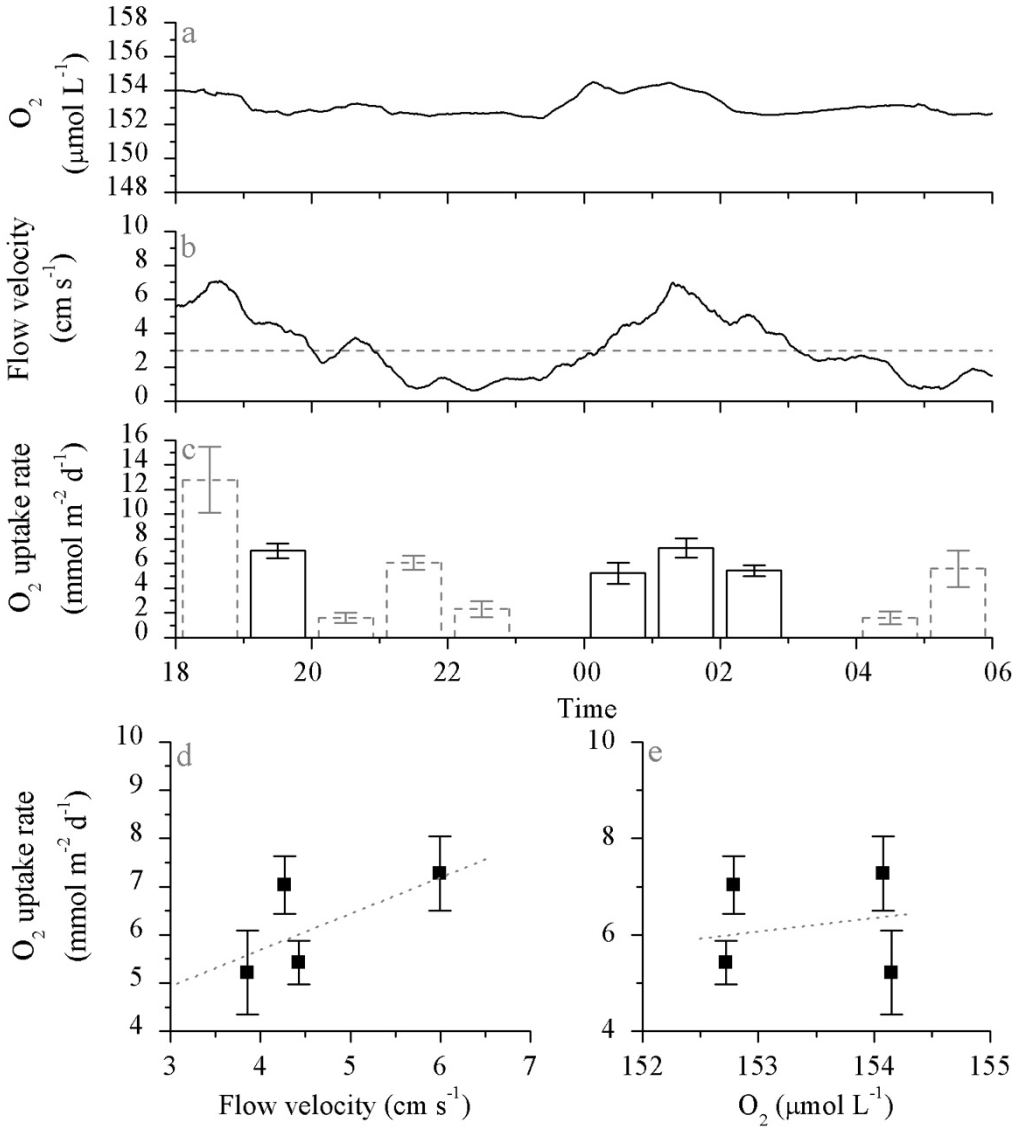
Supplementary Figure 3. Representative in situ O_2 and H_2S concentration profiles from PRFL-1 (a, b) and PRFL-2 (c, d) deployments. Dashed horizontal lines indicate the sediment–water interface (SWI; 0 mm). Well-defined diffusive boundary layers (DBL) were commonly observed, with average thicknesses (δ_{DBL}) of 0.5 ± 0.4 mm for PRFL-1 and 0.5 ± 0.5 mm for PRFL-2. Panel (a) illustrates the determination of δ_{DBL} (thick line and vertical marker) and the oxygen penetration depth (z_{max}). Panel (b) shows the definition of the suboxic zone, extending from z_{max} to the first depth of H_2S detection.



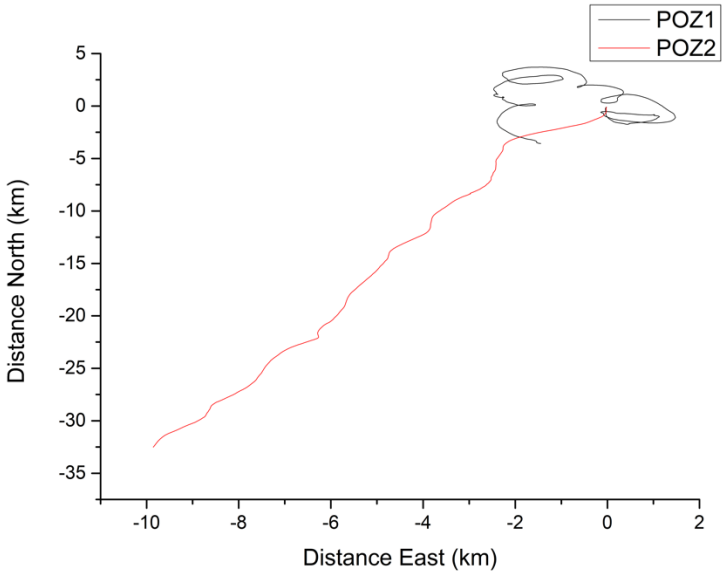
Supplementary Figure 4. Overview of profiler lander measurements for PRFL-1 (a–e) and PRFL-2 (f–j). (a, f) Diffusive oxygen uptake (DOU) derived from O_2 profiles measured by sensor 1 (squares) and sensor 2 (circles). (b, g) Diffusive boundary layer thickness (δ_{DBL}) inferred from O_2 profiles. (c, h) Maximum O_2 penetration depth (z_{max}). (d, i) Flow velocity magnitude. (e, j) Bottom-water O_2 concentrations measured ~18 cm above the sediment. Grey numbers indicate profile number; filled symbols denote H_2S detection for the respective sensor.



Supplementary Figure 5. Overview of benthic O_2 uptake in Box-2 as quantified using the eddy correlation module (ECM). (a) Near-bottom O_2 concentrations measured with a microelectrode and (b) flow velocity magnitude measured with an acoustic Doppler velocimeter (ADV); both datasets are shown as 20-min averages to highlight temporal variability. The dotted line in (b) indicates the minimum flow velocity required to sustain turbulent transport at the site. (c) Benthic O_2 uptake flux rates ($F_{benthic}$; as defined in Suppl. Eq. 4) averaged over 1-h intervals; dashed bars denote values flagged due to insufficient flow or poor data quality. (d, e) Turbulent O_2 uptake rates as a function of (d) flow velocity and (e) near-bottom O_2 concentration; dashed lines indicate linear regressions. The ECM was deployed in Box-2 on soft sediments characterized by patches of white sulfur-oxidizing bacterial mats and blackened reduced sediments.



Supplementary Figure 6. Overview of benthic O_2 uptake in Box-4 quantified using the eddy correlation module (ECM). (a) Near-bottom O_2 concentrations measured with a microelectrode and (b) flow velocity magnitude measured with an acoustic Doppler velocimeter (ADV); both datasets are shown as 20-min averages to highlight temporal variability. The dotted line in (b) indicates the minimum flow velocity required to sustain turbulent transport at the site. (c) Benthic O_2 uptake rates ($F_{benthic}$; as defined in Suppl. Eq. 4) averaged over 1-h intervals; dashed bars denote values flagged due to insufficient flow or poor data quality. (d, e) Turbulent O_2 uptake rates as a function of (d) flow velocity and (e) near-bottom O_2 concentration; dashed lines indicate linear regressions. The ECM was deployed in Box-4 inside the Dead Clam Field.



183

184 **Supplementary Figure 7.** Overview of averaged theoretical particle tracks from the near-sediment currents (2.1 m
185 to ~21.5 m distance). Note that the POZ-1 (Box-2) deployment was almost twice as long as POZ-2 (Box-4).

186

3. Supplementary References

Attard, K. M., Stahl, H., Kamenos, N. A., Turner, G., Burdett, H. L., and Glud, R. N.: Benthic oxygen exchange in a live coralline algal bed and an adjacent sandy habitat: an eddy covariance study, Marine Ecology Progress Series, 535, 99-115, https://doi.org/10.3354/meps11413, 2015.

Berg, P., Røy, H., and Wiberg, P. L.: Eddy correlation flux measurements: The sediment surface area that contributes to the flux, Limnology and Oceanography, 52, 1672-1684, https://doi.org/10.4319/lo.2007.52.4.1672, 2007.

Berg, P., Røy, H., Janssen, F., Meyer, V., Jørgensen, B. B., Huettel, M., and De Beer, D.: Oxygen uptake by aquatic sediments measured with a novel non-invasive eddy-correlation technique, Mar. Ecol. Prog. Ser., 261, 75-83, https://doi.org/10.3354/meps261075, 2003.

Broecker, W. S. and Peng, T.-H.: Gas exchange rates between air and sea, Tellus, 26, 21-35, https://doi.org/10.3402/tellusa.v26i1-2.9733, 1974.

Bryant, L. D., McGinnis, D. F., Lorrai, C., Brand, A., Little, J. C., and Wüest, A.: Evaluating oxygen fluxes using microprofiles from both sides of the sediment-water interface, Limnology and Oceanography: Methods, 8, 610-627, https://doi.org/10.4319/lom.2010.8.0610, 2010.

Donis, D., Holtappels, M., Noss, C., Cathalot, C., Hancke, K., Polsenaere, P., Wenzhöfer, F., Lorke, A., Meysman, F. J., and Glud, R. N.: An assessment of the precision and confidence of aquatic eddy correlation measurements, Journal of Atmospheric and Oceanic Technology, 32, 642-655, https://doi.org/10.1175/JTECH-D-14-00089.1, 2015.

Inoue, T., Glud, R. N., Stahl, H., and Hume, A.: Comparison of three different methods for assessing in situ friction velocity: A case study from Loch Etive, Scotland, Limnology and Oceanography: Methods, 9, 275-287, https://doi.org/10.4319/lom.2011.9.275, 2011.

Jeroschewski, P., Steuckart, C., and Kühl, M.: An amperometric microsensor for the determination of H2S in aquatic environments, Analytical chemistry, 68, 4351-4357, https://doi.org/10.1021/ac960091b, 1996.

Jørgensen, B. B. and Des Marais, D. J.: The diffusive boundary layer of sediments: oxygen microgradients over a microbial mat, Limnology and Oceanography, 35, 1343-1355, https://doi.org/10.4319/lo.1990.35.6.1343, 1990.

Jørgensen, B. B. and Revsbech, N. P.: Diffusive boundary layers and the oxygen uptake of sediments and detritus, Limnol. Oceanogr., 30, 111-122, https://doi.org/10.4319/lo.1985.30.1.0111, 1985.

Lorke, A., McGinnis, D. F., and Mäck, A.: Eddy-correlation measurements of benthic fluxes under complex flow conditions: Effects of coordinate transformations and averaging time scales, Limnology and Oceanography: Methods, 11, 425-437, https://doi.org/10.4319/lom.2013.11.425, 2013.

McGinnis, D. F., Sommer, S., Lorke, A., Glud, R. N., and Linke, P.: Quantifying tidally driven benthic oxygen exchange across permeable sediments: An aquatic eddy correlation study, Journal of Geophysical Research: Oceans, 119, 6918-6932, https://doi.org/10.1002/2014JC010303, 2014.

McGinnis, D. F., Berg, P., Brand, A., Lorrai, C., Edmonds, T. J., and Wüest, A.: Measurements of eddy correlation oxygen fluxes in shallow freshwaters: Towards routine applications and analysis, Geophysical Research Letters, 35, https://doi.org/10.1029/2007GL032747, 2008.

Millero, F. J., Plese, T., and Fernandez, M.: The dissociation of hydrogen sulfide in seawater 1, Limnology and Oceanography, 33, 269-274, https://doi.org/10.4319/lo.1988.33.2.0269, 1988.

Mori, N., Suzuki, T., and Kakuno, S.: Noise of acoustic Doppler velocimeter data in bubbly flows, Journal of engineering mechanics, 133, 122-125, https://doi.org/10.1061/(ASCE)0733-9399(2007)133:1(122), 2007.

Reidenbach, M. A., Monismith, S. G., Koseff, J. R., Yahel, G., and Genin, A.: Boundary layer turbulence and flow structure over a fringing coral reef, Limnology and oceanography, 51, 1956-1968, https://doi.org/10.4319/lo.2006.51.5.1956, 2006.

Rheuban, J. E., Berg, P., and McGlathery, K. J.: Multiple timescale processes drive ecosystem metabolism in eelgrass (Zostera marina) meadows, Marine Ecology Progress Series, 507, 1-13, https://doi.org/10.3354/meps10843, 2014.

Rovelli, L., Attard, K. M., Bryant, L. D., Flögel, S., Stahl, H., Roberts, J. M., Linke, P., and Glud, R. N.: Benthic O2 uptake of two cold-water coral communities estimated with the non-invasive eddy correlation technique, Marine Ecology Progress Series, 525, 97-104, https://doi.org/10.3354/meps11211, 2015.

Stahel, W.: Statistische Datenanalyse: Eine Einführung Für Naturwissenschaftler (Statistical Data Analysis: An Introduction for Scientists), 2002.

Yuan-Hui, L. and Gregory, S.: Diffusion of ions in sea water and in deep-sea sediments, Geochimica et cosmochimica acta, 38, 703-714, 10.1016/0016-7037(74)90145-8, 1974.